Photosensitizers

The Coordination Behaviour of Cu^{I} Photosensitizers Bearing Multidentate Ligands Investigated by X-ray Absorption Spectroscopy

Martin Rentschler,[a] Sirma Iglesias,[b] Marie-Ann Schmid,[c] Cunming Liu,[d] Stefanie Tschierlei,[c] Wolfgang Frey,[a] Xiaoyi Zhang,[d] Michael Karnahl,*[a] and Dooshaye Moonshiram*[b]

Abstract: A systematic series of four novel homo- and heteroleptic Cu^{I} photosensitizers based on tetradentate 1,10-phenanthroline ligands of the type X^N^N^X containing two additional donor moieties in the 2,9-position (X = SMe or OMe) were designed. Their solid-state structures were assessed by X-ray diffraction. Cyclic voltammetry, UV-vis absorption, emission and X-ray absorption spectroscopy were then used to determine their electrochemical, photophysical and structural features in solution. Following, time-resolved X-ray absorption spectroscopy in the picosecond time scale, coupled with time-dependent density functional theory calculations, provided in-depth information on the excited state electron configurations. For the first time, a significant shortening of the Cu–X distance and a change in the coordination mode to a pentacoordinated geometry is shown in the excited states of the two homoleptic complexes. These findings are important with respect to a precise understanding of the excited state structures and a further stabilization of this type of photosensitizers.

Introduction

Considerable attention is currently being paid to develop novel technologies to harvest and to store energy in a sustainable fashion.[1] For instance, the solar light-driven splitting of water for hydrogen fuel production is a promising alternative to fossil fuels due to their rapid depletion and concomitant environmental pollution.[1c,2] Hence, the design of light-driven devices composed of organic, inorganic or hybrid materials that can mimic natural photosynthetic processes is extremely desirable.[3] An essential component of such systems is the light-harvesting chromophore,[4] analogous to the photosynthetic pigments, which can absorb the energy of the incident photons. Consequently, the light energy is converted into an electronically excited state[4f] for the creation of a charge-separated state that helps to generate the required thermodynamic driving force for subsequent catalytic reactions.

Commonly used molecular photosensitizers traditionally contain precious and scarce 4d or 5d transition metals such as Platinum,[5] Ruthenium,[1c,4d,6] Rhenium[7] or Iridium.[1a,4f,8] The widespread application of these compounds is explained by their broad absorption, suitable redox potentials for the required electron transfer to the catalytic centre, sufficiently long excited-state lifetimes and reasonable photostabilities. However, over the past decades, a range of noble metal-free photosensitizers based on earth-abundant metals such as copper,[2c,9] chromium[2b,10] and zinc[2a,4b,11] appeared, with the aim to bring these light-harvesting molecules into more practical applications.[2c,4f,12] In particular, heteroleptic diphosphine-diimine Cu^{I} complexes of the type $[(P\text{^}P)Cu(N\text{^}N)]^{+}$ (where P^P represents a diphosphine and N^N a diimine ligand) received significant attention.[9l,13] These heteroleptic Cu^{I} complexes are especially suited due to the modular nature and great variety of their ligands,[9f,12c,13a,b,14] which can be easily tuned to modify the resulting redox potentials, photostabilities and excited state properties.

[a] M. Rentschler, Dr. W. Frey, Dr. M. Karnahl
Institute of Organic Chemistry
University of Stuttgart
Pfaffenwaldring 55, 70569 Stuttgart (Germany)
E-mail: michael.karnahl@oc.uni-stuttgart.de

[b] S. Iglesias, Dr. D. Moonshiram
Instituto Madrileño de Estudios Avanzados en Nanociencia (IMDEA Nanociencia)
Calle Faraday, 9, 28049 Madrid (Spain)
E-mail: dooshaye.moonshiram@imdea.org

[c] M.-A. Schmid, Dr. S. Tschierlei
Institute of Inorganic Chemistry I
Ulm University
Albert-Einstein-Allee 11, 89081 Ulm (Germany)

[d] Dr. C. Liu, Dr. X. Zhang
X-ray Science Division
Argonne National Laboratory
9700 S. Cass Avenue, Lemont, IL 60439 (USA)

Supporting information and the ORCID identification number(s) for the author(s) of this article can be found under: https://doi.org/10.1002/chem.201905601.

The main aims in the ongoing tailoring of Cu^{I} photosensitizers lie in enhancing the (photo)stability, achieving reversible redox events and in influencing the coordination geometry of the excited states. In the present study the latter issue should be tackled by multidentate diimine ligands, which contain two additional donor sites. This design strategy might enable them to occupy an open coordination site around the Cu centre upon photoexcitation.[13j,k,15]

Towards this goal, two new 1,10-phenanthroline ligands of the type X^N^N^X, that contain two additional donor moieties in 2,9-position (with X = SMe or OMe), were developed to investigate the coordination behaviour of multidentate ligands on the corresponding homo- (**C1** and **C3**) and heteroleptic (**C2** and **C4**) Cu^{I} complexes (Scheme 1). Both, **C2** and **C4**, possess the bulky and rigid xantphos (xant), as this diphosphine ligand was shown to enable beneficial properties such as long-lived excited states resulting in high photocatalytic activities.[2c,9h,l]

A combination of standard characterization techniques including cyclic voltammetry, UV-vis absorption and emission spectroscopy were used to provide a comprehensive analysis of the basic electrochemical and photophysical properties of **C1–C4**. The solid-state structures were assessed through X-ray diffraction (XRD) and their electronic configuration as well as structural conformation in solution were further determined through X-ray absorption near edge structure (XANES) and extended X-ray absorption fine structure analysis (EXAFS). Importantly, time-resolved X-ray absorption spectroscopy (tr-XAS) in the picosecond time regime coupled with time-dependent density functional theory (TD-DFT) calculations was applied to describe the photophysical processes occurring upon conversion of the initial Cu^{I} complexes into the excited states. This multi-method approach provided valuable insights into the role and impact of an additional donor moiety on the excited states of the homoleptic complexes **C1** and **C3** (Scheme 1). Furthermore, comparison of **C2** and **C4** (Scheme 1) with the previously characterized heteroleptic Cu^{I} complex [(xant)Cu(-Me_2phenPh_2)]PF_6 (xant = xantphos and Me_2phenPh_2 = bathocuproine) allowed to evaluate the influence of the additional donor moiety X in terms of their steric and electronic effects. In consequence, this study gains insights into the ground and excited state coordination behaviour of Cu^{I} complexes that contain multidentate ligands.

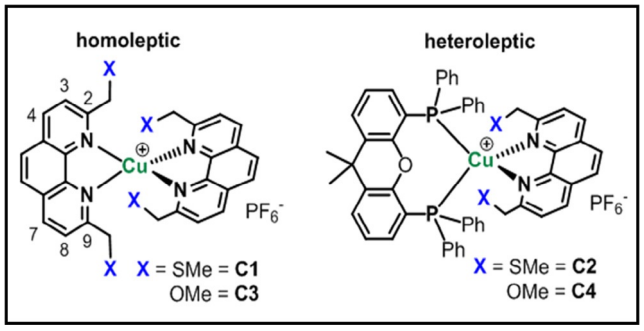

Scheme 1. General structures of the homo- (left) and heteroleptic (right) Cu^{I} complexes **C1–C4** investigated in this study. The numbering on the left side presents the different substituent positions at the 1,10-phenanthroline ligand.

Results and Discussion

Synthesis and structural characterization

The two novel ligands **L1** and **L2** (Scheme 2) were prepared by a two-step procedure. Starting from 2,9-dimethyl-1,10-phenanthroline the 2,9-dibromomethyl-1,10-phenanthroline was synthesized using a literature known protocol.[16] The dibrominated product was then reacted via nucleophilic substitution with sodium thiomethoxide or sodium methoxide, respectively, to yield **L1** and **L2** in 95 and 83% (Scheme 2).

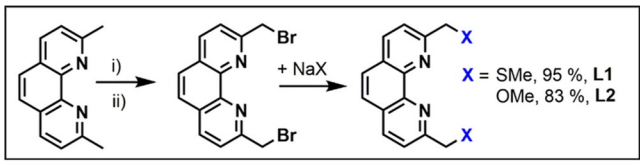

Scheme 2. Preparation of the phenanthroline derived ligands **L1** and **L2** with additional donor functionalities in 2,9-position. Conditions: i) NBS, MeCN, 24 h, reflux and ii) $HPO(OEt)_2$, THF, 24 h, 0 °C to rt.

The homoleptic complexes **C1** and **C3** were subsequently obtained by reacting $[Cu(MeCN)_4]PF_6$ with two equivalents of the respective ligand **L1** and **L2** in dichloromethane solution as previously reported.[12a] The complexes were received as red solids in 81% (**C1**) and 43% yield (**C3**). In contrast, the heteroleptic complexes **C2** and **C4** were synthesized by first introducing the xantphos ligand, followed by slow addition of the corresponding phenanthroline derivative **L1** or **L2** according to a standard method.[2c,9h] As a result, **C2** and **C4** were obtained as yellow solids in 53 and 78% yield, respectively (see the synthesis and characterization details in the Supporting Information).

In a next step, the compositions and structures of all compounds were comprehensively characterized by ^{1}H, ^{13}C, ^{31}P NMR spectroscopy (Figures S1–S4), high resolution mass spectrometry (Figures S5–S8) and elemental analysis. The analytical data obtained are in accordance to the proposed structures (Figure S9 and Table S1). A further characterization of the ground state structures was carried out by using XRD techniques (Figure 1). To this end, suitable single crystals were received for **C2**, **C3** and **C4** by layering a dichloromethane solution of the respective complex with ethanol and *n*-hexane.

The subsequent structural analysis revealed a distorted tetrahedral geometry around the copper centre for all three compounds, which is commonly observed for these types of complexes.[2c,13d,17] The tetrahedral angles of **C2**, **C3** and **C4** demonstrate a significant variation from the ideal tetrahedral angle of 109.5° (Table 1). On the one hand, the homoleptic complex **C3** exhibits slightly larger tetrahedral angles ranging from 110°–140° compared to **C2** and **C4**, which possess a range from 103°–128°. On the other hand, for the heteroleptic complexes **C2** and **C4** the additional donor moieties (SMe or OMe) do not largely impact the structural arrangement. No significant differences were observed compared to the bond lengths and

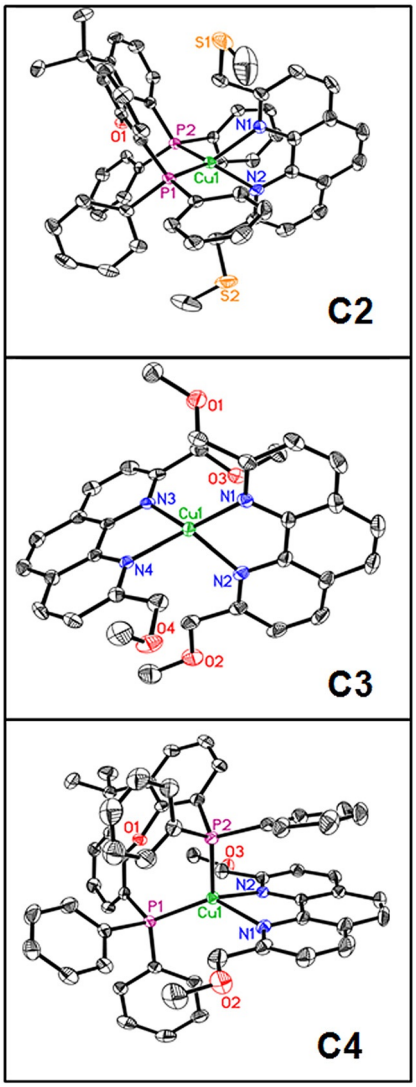

Figure 1. Solid-state structures (ORTEP representation) of the complexes **C2**, **C3** and **C4** (from top to bottom) with thermal ellipsoids at a probability level of 50%. Hydrogen atoms, counter anions and solvent molecules are omitted for clarity.

Table 1. Selected bond lengths (in pm) and angles (in °) of the complexes **C2**, **C3** and **C4** in the solid state (XRD measurements). The respective CCDC reference numbers are 1970787 (**C2**), 1970790 (**C3**) and 1970791 (**C4**).[b]

Homoleptic $[Cu(L)_2]PF_6$	C3	Heteroleptic $[(P\text{^}P)Cu(N\text{^}N)]PF_6$	C2	C4
$Cu–N_1$	201.3(2)	$Cu–N_1$	211.7(4)	211.2(3)
$Cu–N_2$	211.1(2)	$Cu–N_2$	211.1(3)	210.4(2)
$Cu–N_3$	206.2(2)	$Cu–P_1$	225.6(1)	225.7(4)
$Cu–N_4$	204.3(2)	$Cu–P_2$	231.1(1)	229.9(9)
$Cu–X_1$	403.6(2)	$Cu–X_1$	509.1(2)	476.1(3)
$Cu–X_2$	479.3(2)	$Cu–X_2$	473.1(1)	477.8(2)
$Cu–X_3$	316.8(2)			
$Cu–X_4$	465.9(2)			
N_1-Cu-N_2	81.78(9)	N_1-Cu-N_2	79.9(1)	79.7(0)
N_3-Cu-N_4	81.57(8)	P_1-Cu-P_2	115.14(4)	117.14(3)
N_1-Cu-N_3	127.43(9)	N_1-Cu-P_1	119.3(1)	127.84(7)
N_1-Cu-N_4	139.50(9)	N_1-Cu-P_2	106.3(1)	100.58(7)
N_2-Cu-N_3	119.35(9)	N_2-Cu-P_1	129.1(1)	120.94(7)
N_4-Cu-N_4	110.07(8)	N_2-Cu-P_2	100.9(1)	103.05(7)
N-N-N-N[a]	80.35	P-P-N-N[a]	84.53	87.11

The XRD of **C1** was not determined as no single crystals were available. [a] Torsional angle between the two ligand planes. [b] Deposition numbers 1970787 (**C2**), 1970790 (**C3**), and 1970791 (**C4**) contain the supplementary crystallographic data for this paper. These data are provided free of charge by the joint Cambridge Crystallographic Data Centre and Fachinformationszentrum Karlsruhe Access Structures service

angles of the previously reported heteroleptic complex [(xant)-Cu(Me_2phen)]PF_6 (with Me_2phen = 2,9-dimethyl-1,10-phenanthroline, that is, X = H instead of SMe or OMe).[18] Lastly, the crystal structure of **C3** illustrates a slightly more distorted structure than **C2** and **C4**. For instance, **C3** exhibits a torsional angle of 80.35° between the two phenanthroline planes in comparison to the two heteroleptic complexes **C2** and **C4** which only have torsional angles of 84.53° and 87.11°, respectively.

Interestingly, further examination of the bond lengths and angles of **C3** shows that one oxygen atom (i.e. O3, Figure 1) of the OMe group points towards the copper centre, while the three other oxygen donor moieties point away. The respective Cu–O distance (Cu–O3: 316.8(2) pm) is significantly shortened compared to the three other Cu–O distances (403.6(2) to 479.3(2) pm) and indicates that there is a weak interaction between the copper centre and one of the additional donor atoms in the ground state. In contrast, all SMe and OMe donor moieties in the heteroleptic complexes **C2** and **C4** point away from the copper centre maintaining the typical distorted tetrahedral and four-fold coordination.

DFT optimization calculations on the ground state were further carried out using the BP86 functional as elaborated in the supporting information in Figure S14 and Table S2. The averaged theoretically determined Cu–N distances for **C2**, **C3**, and **C4** are 200, 206, and 206 pm (Table S2), respectively, in close agreement with the experimentally determined distances from XRD data analysis (206, 212, and 211 pm for **C2**, **C3** and **C4**, respectively). The theoretically determined Cu–P distances for the heteroleptic complexes **C2** and **C4** further showed Cu–P distances of 222 pm (Table S2), which are in line with the experimentally extracted distances of 225–231 pm for **C2** and **C4** (Table 1). Importantly, the theoretically determined structures for the homoleptic complexes **C1** and **C3** display one shortened Cu–X distance which points towards the copper centre (Figure S14, Figure 4). This is in contrast to the heteroleptic complexes where all the donor moieties point away. The structural orientations and theoretically observed trends observed for the homo- and heteroleptic complexes within the first coordination sphere agree well with data from XRD analysis. This illustrates that the DFT optimization methods can be further employed for the comparison of the local structural conformation of the ground and excited states through EXAFS analysis.

Photophysical and electrochemical characterization

The UV-vis absorption spectra of all complexes display a sharp absorption band around 280 nm (Figure 2), which is attributed

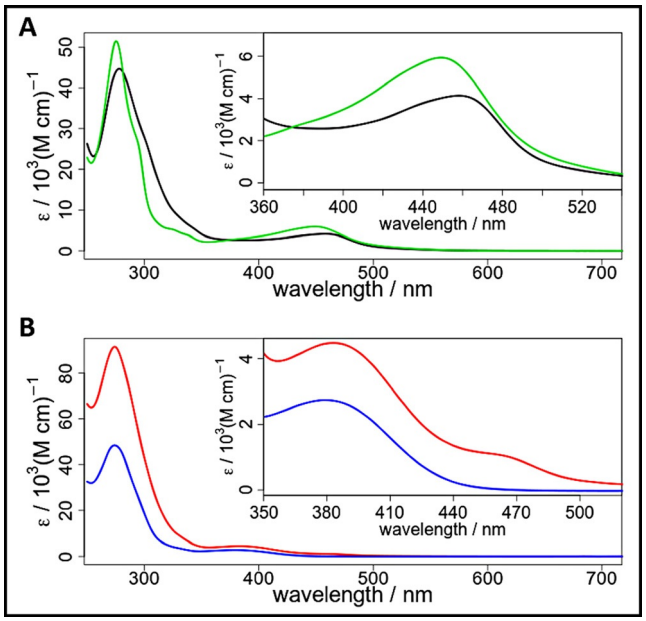

Figure 2. UV-vis spectra (attenuation coefficient) of the **A**. homoleptic complexes **C1** (black) and **C3** (green) in acetonitrile. Inset: Enlargement of the MLCT region. **B**. heteroleptic complexes **C2** (red) and **C4** (blue). Inset: Enlargement of the MLCT region.

to ligand centred (LC) π–π^* transitions.[9i, 19] The metal-to-ligand charge transfer (MLCT) transition band of the two homoleptic complexes is very broad with a maximum at 458 nm (**C1**) and 449 nm (**C3**), respectively (Figure 2). In contrast, the heteroleptic complexes show a compact MLCT transition band with maxima at 379 nm (**C2**) and 384 nm (**C4**). For comparison, the heteroleptic complex [(xant)Cu(Me_2phen)]PF_6 without additional donor substituents has a MLCT maxima of 378 nm.[18] Hence, the impact of the two different donor moieties (i.e. SMe or OMe) on the visible absorption is rather low and it is more crucial whether the complex is homo or heteroleptic. Interestingly, the molar extinction coefficients of the two complexes with SMe groups (**C1** and **C2**, Table 2) are lower than the respective complexes containing the OMe groups (**C3** and **C4**).

On the one hand, the complexes **C1**–**C4** exhibit no emission in deaerated acetonitrile solution (Figure S10). On the other hand, the heteroleptic compounds **C2** and **C4** clearly emit in the solid state, as shown in Figure S11. All complexes also show a very weak emission in tetrahydrofuran (THF) solution (Figure S12).

The electrochemical properties of all four Cu^I complexes were studied by cyclic voltammetry in acetonitrile (Figure S13, Table 2). The heteroleptic complexes **C2** and **C4** each possess one reduction process at −2.03 and −2.04 V vs. Fc/Fc^+, respectively, and three irreversible oxidations. The one electron reduction is irreversible for **C2** (SMe), but reversible for **C4** (OMe). All in all, the reduction potentials and two oxidation potentials of **C2** and **C4** are fairly similar. Only the first oxidation is significantly shifted by 500 mV to lower potentials from **C2** (0.85 V) to **C4** (0.35 V). The observed reduction potentials are also similar to the potentials of structurally related complexes (e.g. $E_{1/2}^{red} = -2.11$ V for [(xant)Cu(Me_2phen)]PF_6).[9l, 19b]

Table 2. Overview of the photophysical and electrochemical properties of the complexes **C1–C4** based on measurements performed in acetonitrile under inert conditions (except UV-vis absorption). Potentials are referenced to the ferrocene/ferricenium (Fc/Fc^+) couple. The emission maxima are detected in the solid state, with an excitation at $\lambda_{abs,MLCT}$.

Complex	$\lambda_{abs,MLCT}$ [nm]	ε_{MLCT} [10^3 (mol·cm)$^{-1}$]	λ_{em} [nm]	$E_{1/2}^{red}$ [V]	$E_{1/2}^{ox}$ [V]
C1	458	4.41	n.d.[b]	−2.19[a]	0.09
				−2.02	1.09
C2	379	2.74	563	−2.03[a]	0.85
					1.04
					1.34[a]
C3	449	5.94	n.d.[b]	−2.22	0.03
				−2.02	
C4	383	4.48	531	−2.04	0.35
					1.03
					1.23

[a] Irreversible peak. [b] Not determined.

The homoleptic complexes have one quasi-reversible oxidation at 0.09 V (**C1**) and 0.03 V (**C3**). The peak separation is broad but becomes smaller at higher scan rates (Figure S14). This could possibly imply a pentacoordinated copper also under electrochemical conditions.[20]

Further, **C1** displays two irreversible reduction peaks (at −2.19 and −2.02 V, Table 2) showing that this complex decomposes during the reduction process. In contrast, **C3** exhibits two reversible reductions (at −2.02 and −2.22 V, Table 2). Both complexes **C3** and **C4**, which contain the 2,9-dimethoxymethyl-1,10-phenanthroline ligand (OMe) have reversible reductions. In contrast, the reduction of the complexes **C1** and **C2** with the 2,9-dithiomethoxymethyl-1,10-phenanthroline ligand (SMe) is always irreversible. From previous studies it is known, that the diimine-ligand (N^N) is reduced and that a [(P^P)Cu^I(N^N^-)] species is formed in such complexes.[2c, 9l] It seems that the methoxy group (OMe) is able to stabilize the reduced (N^N^-) moiety, whereas the thiomethyl group (SMe) is not able to distribute the charge, resulting in ligand decomposition under reductive conditions.

Electronic and structural nature of C1–C4 in solution

To gain more insights into the coordination behaviour and ground state structures of these complexes in solution, steady state XANES and EXAFS measurements were performed in a mixture of THF and water (in a ratio of 9:1). This mixture was chosen to guarantee comparability with our previous results, where [Cu(Me_2phenPh_2)$_2$]PF_6 and [(xant)Cu(Me_2phenPh_2)]PF_6 were studied.[9h, 13l]

The Cu K-edge XANES spectra (Figure 3 A) of Cu^I tetrahedral complexes are generally characterized by a main peak along the rising edge from 8980 to 9000 eV assigned as a $1s \rightarrow 4p_z$ transition.[21] This transition reflects the nature of the $4p_z$ orbital in the pseudotetrahedral coordination environment of these Cu^I complexes.[21a] The homoleptic complexes **C1** and **C3** demonstrate the $1s \rightarrow 4p_z$ transition at 8987 eV, whereas the heteroleptic complexes **C2** and **C4** exhibit this transition at

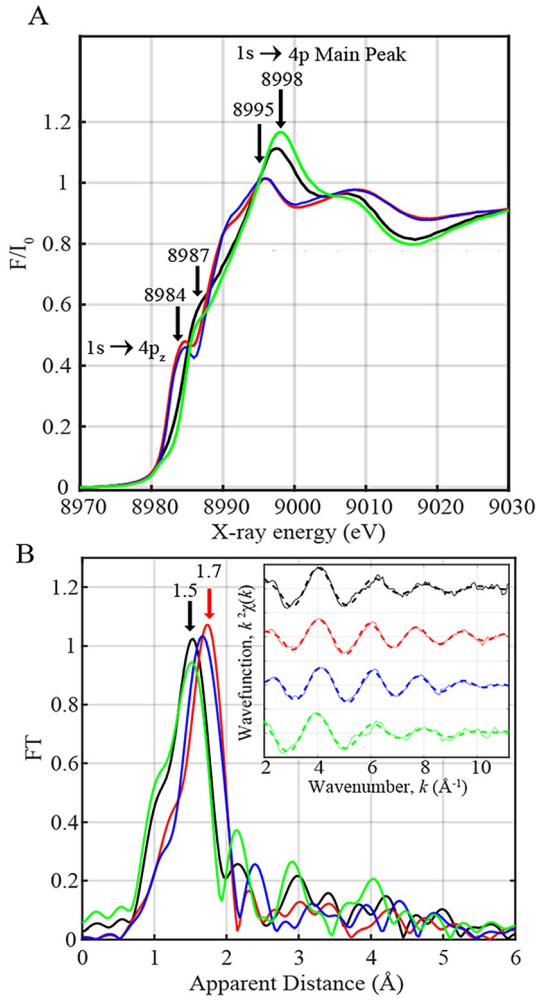

Figure 3. A. Normalized Cu K-edge XANES of **C1** (black), **C2** (red), **C3** (green) and **C4** (blue). **C1** and **C3** are shown in dotted black and green, respectively for better comparisons. **B**. Fourier transforms of k^2-weighted Cu EXAFS for **C1** (black), **C2** (red), **C3** (green) and **C4** (blue). Inset: Back Fourier transformed experimental (solid lines) and fitted (dashed lines) $k^2[\chi(k)]$ of **C1–C4**. Experimental spectra were calculated for k values of 2–11.2 Å^{-1}.

8984 eV. A noticeable pre-edge feature at low photon energies is absent in all complexes (Figure 3 A) as the Cu^{I} complexes have a formal d^{10} electronic configuration with filled e_g and t_{2g} levels. The lack of vacancy in the 3d levels consequently explains the absence of the pre-edge feature in the low energy region around 8980 eV.[22]

Importantly the XANES spectra (Figure 3 A) show small changes in the rising-edge features. This is consistent with the variations observed in the coordination sphere and local symmetry of the four Cu^{I} complexes, as previously indicated through X-ray diffraction analysis.

A prominent peak at apparent distances of 1.5 and 1.7 Å (150 and 170 pm) (Figure 3 B) is observed in the EXAFS spectra of the homo- and heteroleptic complexes, respectively, corresponding to the averaged contribution of the Cu–N/P bond distances. The EXAFS fits for the extraction of the actual bond distances of all four complexes are shown in Figure 3 B inset, Table S4 and Figure S16.

Analysis of the EXAFS spectra in **C1** and **C3** clearly resolves four Cu–N distances of 202 pm (Table S4). Similarly, EXAFS analysis of **C2** and **C4** illustrates improvement of the fit quality with two Cu–N distances at 212 and 209 pm, respectively, in agreement with obtained XRD data (Table S4). In addition, inclusion of two sets of Cu–P distances of 230 pm in **C2** and 228 pm in **C4** improves the quality of the fit significantly as shown by the decreased R-factors and χ^2 values (Table S4, fits 4 and 7). The differences and trends observed in the experimental EXAFS for all four complexes agree well with the local structural data extracted from XRD analysis and EXAFS simulations carried out from DFT optimized coordinates (Table 3, Figure S15). This shows that theoretical methods including geometry optimizations can be reliably used for understanding the structural conformations of the excited state structures of **C1–C4** within the first coordination sphere.

Table 3. Comparison of structural parameters obtained from DFT calculations (Table S2), and EXAFS analysis. Bond lengths are given in pm.

Complex	DFT ground state [pm]	DFT excited state [pm]	EXAFS fits[pm]
C1	Cu–N: 200.5, 200.3, 199.1, 201.7 Cu–S: 364.3	Cu–N: 193.9, 205.6, 205.6, 228.7 Cu–S: 246.9	Ground state: Cu–N: 4×203
C2	Cu–N: 206.3, 205.4 Cu–P: 220.1, 224.0	Cu–N: 200.2, 201.2 Cu–P: 235.0, 235.7 Cu–S: 335.7	Ground state: Cu–N: 2×212 Cu–P: 2×230 Excited state: Cu–N: 2×200 Cu–P: 2×250
C3	Cu–N: 199.3, 199.6, 200.0, 199.5 Cu–O: 335.2	Cu–N: 191.0,198.5, 208.4, 220.9 Cu–O: 228.6	Ground state: Cu–N: 4×203
C4	Cu–N: 206.2, 205.3 Cu–P: 220.4, 223.9	Cu–N: 197.84, 202.77 Cu–P: 234.15, 239.10	Ground state: Cu–N: 2×208 Cu–P: 2×228 Excited state: Cu–N: 2×206 Cu–P: 2×242

Elucidation of the excited-state structures through time-resolved X-ray spectroscopy

Formation of the triplet excited state structures (Figure 4) of the Cu-based photosensitizers was probed in the picosecond time range through time-resolved X-ray spectroscopy. The complexes were optically pumped at 400 nm in the MLCT range and probed with X-ray pulses. XAS spectra were collected both before (laser off) and after (laser on) laser excitation. By subtracting the laser-off from the laser-on spectrum, a transient signal is obtained for each pump-probe delay. The transient spectrum thus provides information about the photo- induced dynamics, electronic and structural nature of the triplet excited states of these Cu-based photosensitizers (Figure 5). The XAS spectra at an averaged time delay of 80 ps between the laser pump excitation and X-ray probing are shown in Figure 5. Upon light excitation, MLCT transition from the 3d orbital of Cu^{I} to the π^* orbital of the ligand accompanied by flattening distortion initially occurs in around 1 ps.[9l,23] This process is subsequently followed by intersystem crossing to a triplet excited state in about 7–10 ps.[9l,23]

A transient signal (Figure 5) with a maximum time-dependent peak energy at 9000 eV is obtained, which is typical[24] for the signature of the formally oxidized "Cu^{II}" excited state. The transient signals of **C1** and **C3** are weaker owing to the lesser degree of changes observed in the 1s to 3d and 4p transitions

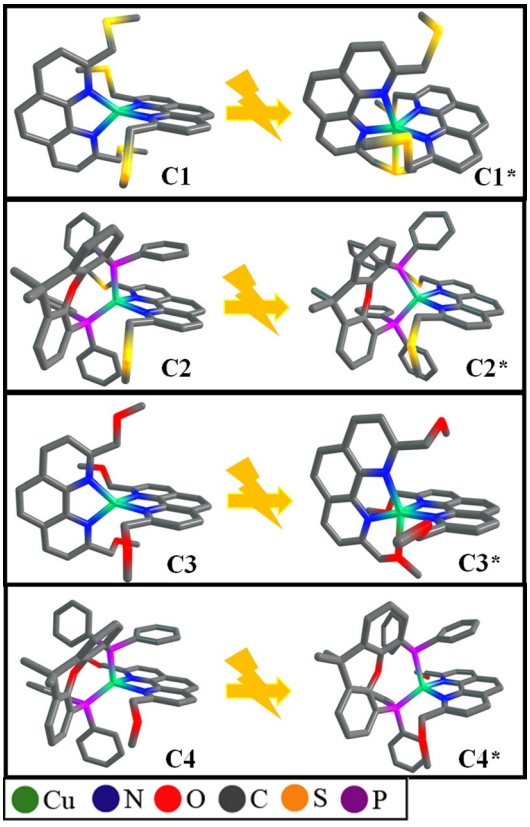

Figure 4. DFT calculated structures of the complexes **C1**–**C4** in the ground (left side) and excited state (right side). Hydrogen atoms are omitted for clarity.

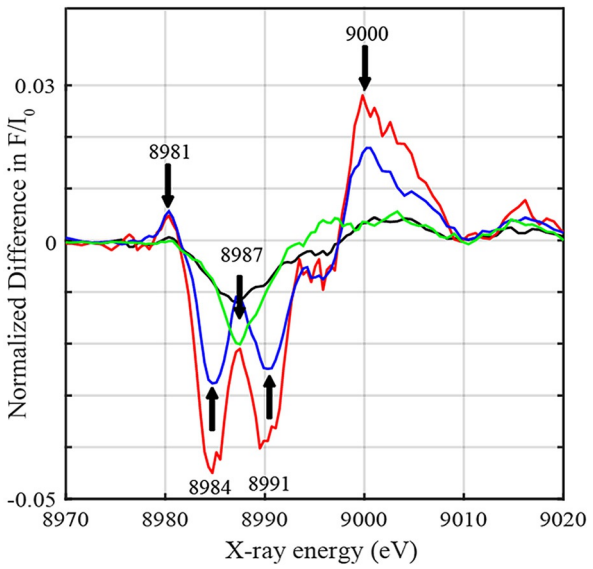

Figure 5. Time-resolved XAS spectra (Laser ON-OFF) corresponding to the excited states of **C1** (black), **C2** (red), **C3** (blue) and **C4** (green) owing to metal-to-ligand charge transfer transitions at a delay of 80 ps between laser and X-ray pulses for a mixture of 1 mM complex in THF/H_2O with a volume ratio of 9:1.

observed between their "laser-on" and "laser-off" spectra at 80 ps.

Interestingly, clear changes are observed in the reduction of the ligand and oxidation of the Cu metal centre as observed by the prominent peak at 9000 eV (Figure 5). Sharp differences are as well observed in the pre-edge and rising-edge transitions of the absorption spectra at lower photon energies between 8981–8991 eV. These features indicate strong changes in the electronic configurations and coordination environment of the "laser-on" spectra of the Cu-based complexes.

Upon light excitation, MLCT transition triggers an electron to be promoted to the low-lying π^* orbital of the ligand,[9l,13k,21c,23b,24a,25] thus causing a change in the d level occupation from $3d^{10}$ to $3d^9$. Thus, the prominent peak observed at 8981 eV is explained by d level atomic rearrangements in the excited state, which are further accompanied with structure relaxation and increased mixing of the valence 3d states with the ligand p orbitals.[22,26] The low-energy pre-edge feature further confirms presence of the formally oxidized "Cu^{II}" state.[21b,c,24b,c]

Two intense transitions at 8984 and 8991 eV (Figure 5) are additionally observed resulting from the changes in the 1s→$4p_z$ and the 1s→4p peak, respectively. These two transitions together with the broad feature at 9000 eV relate to the ground state bleaching of the Cu^{I} ground state along with the formation of the excited state.

Interestingly, the time-resolved XANES spectra of the homoleptic complexes **C1** and **C3** demonstrate a relative decrease in the pre-edge peak in comparison to **C2** and **C4. C1** and **C3** further exhibit a single negative transition peak at 8987 eV. The differences in the pre-edge and 1s→4p transitions observed in the transient signals of **C1** and **C3** vs. **C2** and **C4** (Figure 5) illustrate the clear variations in the electronic and local geomet-

ric configurations of the excited states of the homo- versus the heteroleptic complexes.

Both the decrease in the pre-edge intensity, and broadened bleach peak observed at 8987 eV in **C1** and **C3** correspond to an increase in the coordination number of the copper centre in the excited states of the homoleptic complexes. As previously elaborated, features in the pre-edge region have been shown to be particularly sensitive to the geometry.[15b,21a,26b,27] A decrease in the pre-edge feature was for instance shown to decrease with an increase in the coordination number due to a decrease in the dipole allowed 1s→4p character contributing to this transition.[26b,28] The 1s to $4p_z$ transition moreover reflects the coordination environment of the Cu^I complexes.[21a,22] When the Cu centre is tetracoordinated, the $4p_z$ is localized giving rise to a clear 1s→$4p_z$ transition peak. However, a change in the coordination geometry of the Cu centre leads to a greater delocalization of the metal 4p orbitals, resulting in a broader 1s→$4p_z$ transition feature.[21b,c] The increased coordination number in the excited states of **C1** and **C3** thus leads to a decreased intensity in the pre-edge feature. The single bleach peak observed for **C1** and **C3** at 8987 eV further arises due to the broadened and smeared change in the 1s→$4p_z$ peak transition in their excited state conformations, in comparison to **C2** and **C4**. The experimental changes observed in the transient signals of **C1** and **C3** are further corroborated by theoretical XANES simulations (Figure S18).

The changes in the metal K-rising edge and pre-edge regions of the excited states in combination with our theoretical calculations thus enable the extraction of valuable electronic and geometric structure information about the Cu site (Figure 4). Further, the geometry optimization calculations of the excited states of **C1** and **C3** (Table 3, Figure 4 and Supporting Information) predict a distortion of the local coordination sphere and the presence of an additionally coordinated oxygen or sulfur atoms at 229 and 247 pm, respectively.

It should be mentioned that the excited state fractions of **C1** and **C3** at 80 ps delay between the laser pump excitation and X-ray probing were too low (less than 5%), to reconstruct the EXAFS and structural conformations of the excited states. While the discussion of the times scales of formation of the excited states of **C1–C4** is outside the scope of this manuscript, the decreased excited state fractions of **C1** and **C3** observed at 80 ps could be due to the faster formation of their MLCT states in comparison to **C2** and **C4**. However, both the pre-edge and rising edge features coupled with our TD-DFT XANES calculations and DFT optimizations (Figure S18, Table 3) provide a fingerprint of the local coordination sphere of the MLCT excited states of the homoleptic complexes.

The heteroleptic Cu complexes **C2** and **C4** on the other hand show a clear positive shift of around 0.25 and 0.16 eV (Figures 6 A,C), respectively, at around half height and 0.55 nor-

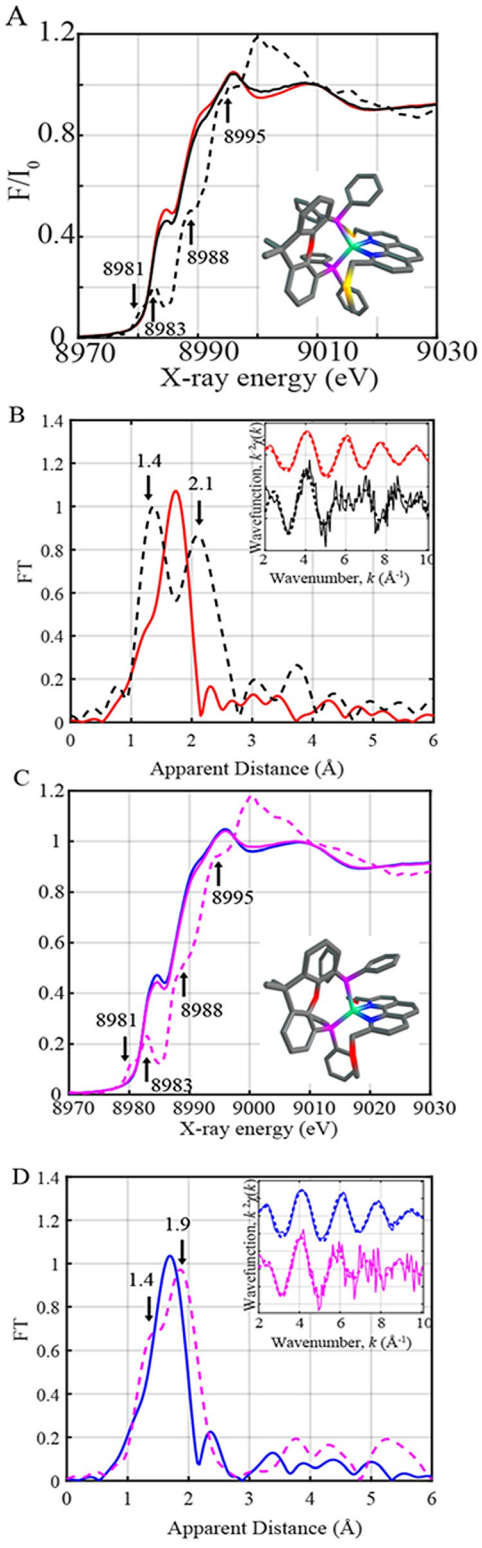

Figure 6. A. Normalized Cu K-edge XANES of the laser off spectrum (in red), laser on (in black), and reconstructed excited state (in dotted black) of **C2** assuming a percentage excited state of ≈12.5%. **B**. Experimental Fourier transforms of k^2-weighted Cu EXAFS of the laser off (in red) and reconstructed excited state (in dotted black) of **C2**. Inset: Back Fourier transformed experimental (solid lines) and fitted (dashed lines) $k^2[\chi(k)]$ of the laser off and reconstructed spectra of **C2**. Experimental spectra were calculated for *k* values of 2–10.097 $Å^{-1}$. **C**. Normalized Cu K-edge XANES of the laser off (in blue), laser on (magenta) and reconstructed excited state spectra of **C4** (dotted magenta) assuming a percentage excited state of around 8%. **D**. Experimental Fourier transforms of k^2-weighted Cu EXAFS of the laser off(blue) and reconstructed excited state (dotted magenta) of **C4**. Inset: Back Fourier transformed experimental (solid lines) and fitted (dashed lines) $k^2[\chi(k)]$ of the laser off and reconstructed excited state of **C4**. Experimental spectra were again calculated for *k* values of 2–10.097 $Å^{-1}$.

malized absorption. The excited state fractions of these two sets of complexes were determined by comparing the relative shift in energy between the theoretically calculated XANES (Figure S19). A relative chemical shift in energy of around 2 eV is obtained between the calculated ground and excited states for **C2** and **C4** (Figure S19), such that a proportion of the excited state of around 12.5 and 8% were estimated in the laser on spectra and further used to plot the actual or reconstructed spectra.

The reconstructed excited states of **C2** and **C4** (Figures 6A,C) exhibit a broad and intense pre-edge transition at 8981–8983 eV and a 1s→4p rising-edge transition at 8988 eV. These features were previously observed for four-fold coordinated Cu^{II} ions.[13l,29] This analysis thus confirms the correct percentage of excited state fraction used in the estimation of the laser on spectra of the heteroleptic photosensitizers described here. The derived excited state of **C2** shows two prominent peaks at apparent distances of 140 and 210 pm whereas that of **C4** reveal two peaks at 140 and 190 pm (Figures 6B,D). These two features correspond to the distinct contributions of the shortened Cu–N and elongated Cu–P bonds. Similar features were observed for the heteroleptic $[(xant)Cu(Me_2phenPh_2)]PF_6$ complex.[13l] Analysis of the EXAFS peaks within the first coordination sphere of the triplet excited states (Table 3, Table S4, Figure S17) clearly resolves the decreased Cu–N bond lengths at 200 and 206 pm for **C2** and **C4**, respectively. Furthermore, the inclusion of two Cu-P bond distances at 250 and 242 pm (Table S4) improve the quality of the fit considerably as shown by the decreased R-factors and reduced χ^2 values (Fits 9 and 11, Table S4). The EXAFS fit values are in good agreement with DFT optimizations (Table 3, Table S4).

As previously elaborated, the structural changes of the excited states provide a strong indication for the dissociation of the diphosphine ligand and a possible degradation pathway of such heteroleptic copper photosensitizers.[13l] The elongation of the Cu–P distances in the triplet excited states of **C2** and **C4** could lead to a stepwise decomposition of these heteroleptic complexes and the formation of their homoleptic counterparts during photocatalysis.[14e,19b,30]

Conclusions

By using a combination of XRD, time-resolved XANES and EXAFS measurements the ground and excited state structures of four novel homo- and heteroleptic copper photosensitizers were systematically elucidated in the solid state and in solution. The experimental results were further supported by theoretical XANES and TD-DFT calculations. Most importantly, these methods were used to evaluate the influence of additional donor moieties (i.e. SMe or OMe) at the phenanthroline ligand on the resulting structures of the Cu^{I} complexes. Indeed, the time-resolved XANES measurements and theoretical simulations illustrate a significant distortion of the local coordination sphere in the excited state structures of the homoleptic complexes **C1** and **C3**. They also evidenced the formation of a penta-coordinated copper centre in the excited state, corresponding to a 4+1-fold coordination mode. This additional coordination of a third donor is in strong contrast to the usual fourfold coordination of Cu^{I} in the ground state. In the future, this observation might lead to the design of improved multidentate ligands with bulkier substituents that can adopt a similar penta-coordinated geometry in the excited state, and thus, help to prevent flattening distortion and intermolecular nucleophilic attack by solvent molecules or counter ions at the copper centre.

Further, time-resolved XANES and EXAFS analysis of the heteroleptic complexes **C2** and **C4** revealed a decrease in the Cu–N and an increase in the Cu–P distances of the excited state structures. The increase in the Cu–P bond distances in the excited state explains the absence of a penta-coordinated arrangement in the heteroleptic complexes in comparison to the homoleptic ones. Importantly, the elongation of the Cu–P distances in the triplet excited states of the heteroleptic complexes **C2** and **C4** provides a clear indication for the dissociation pathway of such diphosphine ligands and the stepwise transformation into their homoleptic counterparts during photocatalysis. Comparison of **C2** and **C4** with previously studied heteroleptic Cu^{I} photosensitizers also emphasize the need to implement bulkier substituents than SMe or OMe at the 2,9-position of the 1,10-phenanthroline. The introduction of additional donor moieties at the terminal ends of tetra- or bidentate ligands are also essential for stabilizing the local coordination geometry and for increasing the steric demand.

Further fine-tuning possibilities, which are currently in progress, involve the implementation of SR and OR (with for example, R = Ph or *i*Pr) substituents that affect the rigidity, bulkiness, bite angle and electronic impact. Beyond this also the incorporation of additional phosphine donors PR or the direct connection of a diimine with a diphosphine seems promising. This might open up the way to improved copper photosensitizers in the future that challenge traditional noble metal complexes for photocatalytic applications.

Acknowledgements

This work was supported by the Severo Ochoa Excellence program (SEV-2016-0686 from the Instituto IMDEA Nanociencia), the Acciones de Dinamización Europa Investigacion grant (EIN2019-103399), the Spanish Ministerio de Ciencia, Innovación y Universidades grant (PID2019-111086RA-I00), the Baden-Württemberg Foundation (BW-Stiftung, Germany), the Deutsche Forschungsgemeinschaft (DFG) within the Priority Program SPP 2102 "Light-controlled reactivity of metal complexes" (TS 330/4-1 and KA 4671/2-1), and the DFG project TS 330/3-1. S.I. acknowledges funding from the Ayudante de Investigacion grant ref. PEJ-2019-AI/AMB-13038 from the Comunidad de Madrid. The DFT calculations were carried out on the CCC cluster (CATDesign Project, PI: D.Moonshiram) at the Universidad Autónoma de Madrid. This research also used resources of the Advanced Photon Source (Beamline 11 ID-D), a U.S. DOE Office of Science User Facility operated for the DOE Office of Science by Argonne National Laboratory under Contract No. DE-AC02-06CH11357.

Conflict of interest

The authors declare no conflict of interest.

Keywords: copper photosensitizers · density functional calculations · excited state structures · multidentate ligands · X-ray absorption spectroscopy

[1] a) P. Zhang, M. Wang, Y. Na, X. Li, Y. Jiang, L. Sun, *Dalton Trans.* **2010**, *39*, 1204 – 1206; b) N. Queyriaux, R. T. Jane, J. Massin, V. Artero, M. Chavarot-Kerlidou, *Coord. Chem. Rev.* **2015**, *304 – 305*, 3 – 19; c) C. R. Bock, T. J. Meyer, D. G. Whitten, *J. Am. Chem. Soc.* **1975**, *97*, 2909 – 2911; d) C. Acar, I. Dincer, G. F. Naterer, *Int. J. Energy Res.* **2016**, *40*, 1449 – 1473; e) R. E. Smalley, *MRS Bull.* **2005**, *30*, 412 – 417; f) Q. Schiermeier, J. Tollefson, T. Scully, A. Witze, O. Morton, *Nature* **2008**, *454*, 816 – 823.

[2] a) I. Okura, T. Kita, S. Aono, N. Kaji, *J. Mol. Catal.* **1985**, *32*, 361 – 363; b) M. J. Silvero, W. J. Peláez, P. F. Garcia, G. A. Argüello, *RSC Adv.* **2014**, *4*, 15507 – 15510; c) E. Mejía, S.-P. Luo, M. Karnahl, A. Friedrich, S. Tschierlei, A.-E. Surkus, H. Junge, S. Gladiali, S. Lochbrunner, M. Beller, *Chem. Eur. J.* **2013**, *19*, 15972 – 15978; d) N. Armaroli, V. Balzani, *Angew. Chem. Int. Ed.* **2007**, *46*, 52 – 66; *Angew. Chem.* **2007**, *119*, 52 – 67; e) N. Armaroli, V. Balzani, *Chem. Eur. J.* **2016**, *22*, 32 – 57; f) L. Hammarström, *Chem* **2016**, *1*, 515 – 518.

[3] a) N. S. Lewis, D. G. Nocera, *Proc. Natl. Acad. Sci. USA* **2006**, *103*, 15729 – 15735; b) A. Magnuson, M. Anderlund, O. Johansson, P. Lindblad, R. Lomoth, T. Polivka, S. Ott, K. Stensjö, S. Styring, V. Sundström, L. Hammarström, *Acc. Chem. Res.* **2009**, *42*, 1899 – 1909; c) T. S. Teets, D. G. Nocera, *Chem. Commun.* **2011**, *47*, 9268 – 9274; d) P. D. Frischmann, K. Mahata, F. Wurthner, *Chem. Soc. Rev.* **2013**, *42*, 1847 – 1870; e) S. Bensaid, G. Centi, E. Garrone, S. Perathoner, G. Saracco, *ChemSusChem* **2012**, *5*, 500 – 521.

[4] a) W. Zhang, J. Hong, J. Zheng, Z. Huang, J. Zhou, R. Xu, *J. Am. Chem. Soc.* **2011**, *133*, 20680 – 20683; b) T. Lazarides, T. McCormick, P. Du, G. Luo, B. Lindley, R. Eisenberg, *J. Am. Chem. Soc.* **2009**, *131*, 9192 – 9194; c) T. M. McCormick, B. D. Calitree, A. Orchard, N. D. Kraut, F. V. Bright, M. R. Detty, R. Eisenberg, *J. Am. Chem. Soc.* **2010**, *132*, 15480 – 15483; d) M. Kirch, J.-M. Lehn, J.-P. Sauvage, *Helv. Chim. Acta Helv. Chim. Acta.* **1979**, *62*, 1345 – 1384; e) M. Schulz, M. Karnahl, M. Schwalbe, J. G. Vos, *Coord. Chem. Rev.* **2012**, *256*, 1682 – 1705; f) Y.-J. Yuan, Z.-T. Yu, D.-Q. Chen, Z.-G. Zou, *Chem. Soc. Rev.* **2017**, *46*, 603 – 631.

[5] a) J. Kiwi, M. Graetzel, *J. Am. Chem. Soc.* **1979**, *101*, 7214 – 7217; b) X. Wang, S. Goeb, Z. Ji, N. A. Pogulaichenko, F. N. Castellano, *Inorg. Chem.* **2011**, *50*, 705 – 707; c) P. Du, J. Schneider, G. Luo, W. W. Brennessel, R. Eisenberg, *Inorg. Chem.* **2009**, *48*, 4952 – 4962.

[6] a) A. Juris, V. Balzani, P. Belser, A. von Zelewsky, *Helv. Chim. Acta* **1981**, *64*, 2175 – 2182; b) C. R. Bock, J. A. Connor, A. R. Gutierrez, T. J. Meyer, D. G. Whitten, B. P. Sullivan, J. K. Nagle, *J. Am. Chem. Soc.* **1979**, *101*, 4815 – 4824; c) V. Balzani, A. Juris, *Coord. Chem. Rev.* **2001**, *211*, 97 – 115.

[7] B. Probst, C. Kolano, P. Hamm, R. Alberto, *Inorg. Chem.* **2009**, *48*, 1836 – 1843.

[8] a) D. R. Whang, K. Sakai, S. Y. Park, *Angew. Chem. Int. Ed.* **2013**, *52*, 11612 – 11615; *Angew. Chem.* **2013**, *125*, 11826 – 11829; b) F. Gärtner, B. Sundararaju, A.-E. Surkus, A. Boddien, B. Loges, H. Junge, P. H. Dixneuf, M. Beller, *Angew. Chem. Int. Ed.* **2009**, *48*, 9962 – 9965; *Angew. Chem.* **2009**, *121*, 10147 – 10150; c) D. Hollmann, F. Gärtner, R. Ludwig, E. Barsch, H. Junge, M. Blug, S. Hoch, M. Beller, A. Brückner, *Angew. Chem. Int. Ed.* **2011**, *50*, 10246 – 10250; *Angew. Chem.* **2011**, *123*, 10429 – 10433; d) F. Gärtner, A. Boddien, E. Barsch, K. Fumino, S. Losse, H. Junge, D. Hollmann, A. Brückner, R. Ludwig, M. Beller, *Chem. Eur. J.* **2011**, *17*, 6425 – 6436.

[9] a) D. Volz, D. M. Zink, T. Bocksrocker, J. Friedrichs, M. Nieger, T. Baumann, U. Lemmer, S. Bräse, *Chem. Mater.* **2013**, *25*, 3414 – 3426; b) C. S. Smith, C. W. Branham, B. J. Marquardt, K. R. Mann, *J. Am. Chem. Soc.* **2010**, *132*, 14079 – 14085; c) T. Bessho, E. C. Constable, M. Graetzel, A. Hernandez Redondo, C. E. Housecroft, W. Kylberg, M. K. Nazeeruddin, M. Neuburger, S. Schaffner, *Chem. Commun.* **2008**, 3717 – 3719; d) B. Bozic-Weber, S. Y. Brauchli, E. C. Constable, S. O. Fürer, C. E. Housecroft, F. J. Malzner, I. A. Wright, J. A. Zampese, *Dalton Trans.* **2013**, *42*, 12293 – 12308; e) T. E. Hewat, L. J. Yellowlees, N. Robertson, *Dalton Trans.* **2014**, *43*, 4127 – 4136; f) C. J. Martin, B. Bozic-Weber, E. C. Constable, T. Glatzel, C. E. Housecroft, I. A. Wright, *J. Phys. Chem. C* **2014**, *118*, 16912 – 16918; g) L. N. Ashbrook, C. M. Elliott, *J. Phys. Chem. C* **2013**, *117*, 3853 – 3864; h) S.-P. Luo, E. Mejía, A. Friedrich, A. Pazidis, H. Junge, A.-E. Surkus, R. Jackstell, S. Denurra, S. Gladiali, S. Lochbrunner, M. Beller, *Angew. Chem. Int. Ed.* **2013**, *52*, 419 – 423; *Angew. Chem.* **2013**, *125*, 437 – 441; i) M. Karnahl, E. Mejia, N. Rockstroh, S. Tschierlei, S.-P. Luo, K. Grabow, A. Kruth, V. Bruser, H. Junge, S. Lochbrunner, M. Beller, *ChemCatChem* **2014**, *6*, 82 – 86; j) M. Sandroni, Y. Pellegrin, F. Odobel, *C. R. Chim.* **2016**, *19*, 79 – 93; k) M. S. Lazorski, F. N. Castellano, *Polyhedron* **2014**, *82*, 57 – 70; l) Y. Zhang, M. Schulz, M. Wächtler, M. Karnahl, B. Dietzek, *Coord. Chem. Rev.* **2018**, *356*, 127 – 146.

[10] a) L. A. Büldt, O. S. Wenger, *Angew. Chem. Int. Ed.* **2017**, *56*, 5676 – 5682; *Angew. Chem.* **2017**, *129*, 5770 – 5776; b) S. Otto, M. Dorn, C. Förster, M. Bauer, M. Seitz, K. Heinze, *Coord. Chem. Rev.* **2018**, *359*, 102 – 111.

[11] a) K. Kalyanasundaram, M. Grätzel, *Helv. Chim. Acta* **1980**, *63*, 478 – 485; b) L.-C. Song, L.-X. Wang, M.-Y. Tang, C.-G. Li, H.-B. Song, Q.-M. Hu, *Organometallics* **2009**, *28*, 3834 – 3841.

[12] a) C. E. McCusker, F. N. Castellano, *Inorg. Chem.* **2013**, *52*, 8114 – 8120; b) H. Takeda, K. Ohashi, A. Sekine, O. Ishitani, *J. Am. Chem. Soc.* **2016**, *138*, 4354 – 4357; c) R. C. Elder, M. C. Hill, *Inorg. Chem.* **1979**, *18*, 729 – 732.

[13] a) J. Kim, D. R. Whang, S. Y. Park, *ChemSusChem* **2017**, *10*, 1883 – 1886; b) J. Windisch, M. Orazietti, P. Hamm, R. Alberto, B. Probst, *ChemSusChem* **2016**, *9*, 1719 – 1726; c) S. Saeedi, C. Xue, B. J. McCullough, S. E. Roe, B. J. Neyhouse, T. A. White, *ACS Appl. Energy Mater.* **2019**, *2*, 131 – 143; d) E. Leoni, J. Mohanraj, M. Holler, M. Mohankumar, I. Nierengarten, F. Monti, A. Sournia-Saquet, B. Delavaux-Nicot, J.-F. Nierengarten, N. Armaroli, *Inorg. Chem.* **2018**, *57*, 15537 – 15549; e) W. Luo, P. Gobbo, C. D. McNitt, D. A. Sutton, V. V. Popik, M. S. Workentin, *Chem. Eur. J.* **2017**, *23*, 1052 – 1059; f) Y. Zhang, P. Traber, L. Zedler, S. Kupfer, S. Gräfe, M. Schulz, W. Frey, M. Karnahl, B. Dietzek, *Phys. Chem. Chem. Phys.* **2018**, *20*, 24843 – 24857; g) I. Nohara, A. Prescimone, E. C. Housecroft, C. E. Constable, *Inorganics* **2020**, *8*, 4; h) M.-A. Schmid, M. Rentschler, W. Frey, S. Tschierlei, M. Karnahl, *Inorganics* **2018**, *6*, 134; i) M. Alkan-Zambada, S. Keller, L. Martínez-Sarti, A. Prescimone, J. M. Junquera-Hernández, E. C. Constable, H. J. Bolink, M. Sessolo, E. Ortí, C. E. Housecroft, *J. Mater. Chem. C* **2018**, *6*, 8460 – 8471; j) N. S. Murray, S. Keller, E. C. Constable, C. E. Housecroft, M. Neuburger, A. Prescimone, *Dalton Trans.* **2015**, *44*, 7626 – 7633; k) N. Armaroli, *Chem. Soc. Rev.* **2001**, *30*, 113 – 124; l) D. Moonshiram, P. Garrido-Barros, C. Gimbert-Suriñach, A. Picón, C. Liu, X. Zhang, M. Karnahl, A. Llobet, *Chem. Eur. J.* **2018**, *24*, 6464 – 6472.

[14] a) M. Okamura, M. Kondo, R. Kuga, Y. Kurashige, T. Yanai, S. Hayami, V. K. K. Praneeth, M. Yoshida, K. Yoneda, S. Kawata, S. Masaoka, *Nature* **2016**, *530*, 465; b) K. Saito, T. Arai, N. Takahashi, T. Tsukuda, T. Tsubomura, *Dalton Trans.* **2006**, 4444 – 4448; c) M. Sandroni, M. Kayanuma, M. Rebarz, H. Akdas-Kilig, Y. Pellegrin, E. Blart, H. Le Bozec, C. Daniel, F. Odobel, *Dalton Trans.* **2013**, *42*, 14628 – 14638; d) S.-M. Kuang, D. G. Cuttell, D. R. McMillin, P. E. Fanwick, R. A. Walton, *Inorg. Chem.* **2002**, *41*, 3313 – 3322; e) A. Kaeser, M. Mohankumar, J. Mohanraj, F. Monti, M. Holler, J.-J. Cid, O. Moudam, I. Nierengarten, L. Karmazin-Brelot, C. Duhayon, B. Delavaux-Nicot, N. Armaroli, J.-F. Nierengarten, *Inorg. Chem.* **2013**, *52*, 12140 – 12151; f) M. Nishikawa, D. Kakizoe, Y. Saito, T. Ohishi, T. Tsubomura, *Bull. Chem. Soc. Jpn.* **2017**, *90*, 286 – 288; g) C. L. Linfoot, M. J. Leitl, P. Richardson, A. F. Rausch, O. Chepelin, F. J. White, H. Yersin, N. Robertson, *Inorg. Chem.* **2014**, *53*, 10854 – 10861; h) K. Soulis, C. Gourlaouen, C. Daniel, A. Quatela, F. Odobel, E. Blart, Y. Pellegrin, *Polyhedron* **2018**, *140*, 42 – 50; i) A. J. J. Lennox, S. Fischer, M. Jurrat, S.-P. Luo, N. Rockstroh, H. Junge, R. Ludwig, M. Beller, *Chem. Eur. J.* **2016**, *22*, 1233 – 1238; j) M. D. Weber, M. Viciano-Chumillas, D. Armentano, J. Cano, R. D. Costa, *Dalton Trans.* **2017**, *46*, 6312 – 6323.

[15] a) M. Iwamura, S. Takeuchi, T. Tahara, *Acc. Chem. Res.* **2015**, *48*, 782 – 791; b) M. W. Mara, K. A. Fransted, L. X. Chen, *Coord. Chem. Rev.* **2015**, *282 – 283*, 2 – 18; c) T. J. Zerk, P. V. Bernhardt, *Coord. Chem. Rev.* **2018**, *375*, 173 – 190.

[16] D. J. Hernández, H. Vázquez-Lima, P. Guadarrama, D. Martínez-Otero, I. Castillo, *Tetrahedron Lett.* **2013**, *54*, 4930 – 4933.

[17] R. Giereth, W. Frey, H. Junge, S. Tschierlei, M. Karnahl, *Chem. Eur. J.* **2017**, *23*, 17432 – 17437.

[18] M. Heberle, S. Tschierlei, N. Rockstroh, M. Ringenberg, W. Frey, H. Junge, M. Beller, S. Lochbrunner, M. Karnahl, *Chem. Eur. J.* **2017**, *23*, 312 – 319.
[19] a) G. J. Hedley, A. Ruseckas, I. D. W. Samuel, *J. Phys. Chem. A* **2010**, *114*, 8961 – 8968; b) Y. Zhang, M. Heberle, M. Wachtler, M. Karnahl, B. Dietzek, *RSC Adv.* **2016**, *6*, 105801 – 105805.
[20] a) S. M. G. Leite, L. M. P. Lima, S. Gama, F. Mendes, M. Orio, I. Bento, A. Paulo, R. Delgado, O. Iranzo, *Inorg. Chem.* **2016**, *55*, 11801 – 11814; b) V. M. Leovac, M. V. Rodić, L. S. Jovanović, M. D. Joksović, T. Stanojković, M. Vujčić, D. Sladić, V. Marković, L. S. Vojinović-Ješić, *Eur. J. Inorg. Chem.* **2015**, 882 – 895; c) D. B. Rorabacher, *Chem. Rev.* **2004**, *104*, 651 – 698.
[21] a) E. I. Solomon, R. K. Szilagyi, S. DeBeer George, L. Basumallick, *Chem. Rev.* **2004**, *104*, 419 – 458; b) L. X. Chen, G. Jennings, T. Liu, D. J. Gosztola, J. P. Hessler, D. V. Scaltrito, G. J. Meyer, *J. Am. Chem. Soc.* **2002**, *124*, 10861 – 10867; c) L. X. Chen, G. B. Shaw, I. Novozhilova, T. Liu, G. Jennings, K. Attenkofer, G. J. Meyer, P. Coppens, *J. Am. Chem. Soc.* **2003**, *125*, 7022 – 7034.
[22] M. L. Baker, M. W. Mara, J. J. Yan, K. O. Hodgson, B. Hedman, E. I. Solomon, *Coord. Chem. Rev.* **2017**, *345*, 182 – 208.
[23] a) M. Iwamura, H. Watanabe, K. Ishii, S. Takeuchi, T. Tahara, *J. Am. Chem. Soc.* **2011**, *133*, 7728 – 7736; b) S. Tschierlei, M. Karnahl, N. Rockstroh, H. Junge, M. Beller, S. Lochbrunner, *ChemPhysChem* **2014**, *15*, 3709 – 3713.
[24] a) M. Chergui, E. Collet, *Chem. Rev.* **2017**, *117*, 11025 – 11065; b) T. J. Penfold, S. Karlsson, G. Capano, F. A. Lima, J. Rittmann, M. Reinhard, M. H. Rittmann-Frank, O. Braem, E. Baranoff, R. Abela, I. Tavernelli, U. Rothlisberger, C. J. Milne, M. Chergui, *J. Phys. Chem. A* **2013**, *117*, 4591 – 4601; c) G. Smolentsev, A. V. Soldatov, L. X. Chen, *J. Phys. Chem. A* **2008**, *112*, 5363 – 5367.
[25] J. V. Lockard, S. Kabehie, J. I. Zink, G. Smolentsev, A. Soldatov, L. X. Chen, *J. Phys. Chem. B* **2010**, *114*, 14521 – 14527.
[26] a) R. Sarangi, *Coord. Chem. Rev.* **2013**, *257*, 459 – 472; b) T. E. Westre, P. Kennepohl, J. G. DeWitt, B. Hedman, K. O. Hodgson, E. I. Solomon, *J. Am. Chem. Soc.* **1997**, *119*, 6297 – 6314.
[27] M. Sano, S. Komorita, H. Yamatera, *Inorg. Chem.* **1992**, *31*, 459 – 463.
[28] a) D. Moonshiram, C. Gimbert-Suriñach, A. Guda, A. Picon, C. S. Lehmann, X. Zhang, G. Doumy, A. M. March, J. Benet Buchholz, A. Soldatov, A. Llobet, S. H. Southworth, *J. Am. Chem. Soc.* **2016**, *138*, 10586 – 10596; b) D. Moonshiram, A. Guda, L. Kohler, A. Picon, S. Guda, C. S. Lehmann, X. Zhang, S. H. Southworth, K. L. Mulfort, *J. Phys. Chem. C* **2016**, *120*, 20049 – 20057.
[29] a) L. S. Kau, D. J. Spira-Solomon, J. E. Penner-Hahn, K. O. Hodgson, E. I. Solomon, *J. Am. Chem. Soc.* **1987**, *109*, 6433 – 6442; b) N. C. Tomson, K. D. Williams, X. Dai, S. Sproules, S. DeBeer, T. H. Warren, K. Wieghardt, *Chem. Sci.* **2015**, *6*, 2474 – 2487.
[30] S. Fischer, D. Hollmann, S. Tschierlei, M. Karnahl, N. Rockstroh, E. Barsch, P. Schwarzbach, S.-P. Luo, H. Junge, M. Beller, S. Lochbrunner, R. Ludwig, A. Brückner, *ACS Catal.* **2014**, *4*, 1845 – 1849.

Manuscript received: December 11, 2019
Revised manuscript received: February 20, 2020
Accepted manuscript online: March 12, 2020
Version of record online: July 8, 2020

